

# CHAOS INDICATORS FOR STUDYING DYNAMIC APERTURE IN THE IOTA RING WITH PROTONS\*

Kilean Hwang<sup>†</sup>, Chad Mitchell, Robert Ryne  
Lawrence Berkeley National Laboratory, Berkeley, USA

## Abstract

The Integrable Optics Test Accelerator (IOTA) is a novel storage ring under commissioning at Fermi National Accelerator Laboratory designed (in part) to investigate the dynamics of beams in the presence of highly nonlinear transverse focusing fields that generate integrable single-particle motion. In this study, we explore the sensitivity of the lattice dynamic aperture in the presence of nonlinear space-charge. For this purpose, two distinct chaos indicators are compared (frequency map analysis and forward-backward integration). Because the integrability of motion requires integer betatron tune advance between passes out of the nonlinear magnetic element, a large role is played by space-charge-induced tune spread. As a result, these tools are also applied to a toy model of the IOTA lattice to investigate the sensitivity of dynamic aperture to violations of the integer tune advance condition.

## MOTIVATION

In one of the IOTA operation mode, a special nonlinear magnet is inserted so that single particle transverse dynamics is highly nonlinear but integrable [1, 2]. Small perturbation like the space-charge force can destroy some of invariant tori thereby limiting the dynamic aperture. However, studying dynamic aperture with space-charge requires heavy numerical loads including large number of particles, field discretization modes and revolutions over the ring. In this proceeding, we solve such a difficulty with two approaches. One is to model the space-charge effect by a simplified toy model to represent space-charge induced tune depression. The other one is to use an relatively faster chaos indicator ‘forward-backward (FB) integration’ and compare it with the frequency map analysis [3].

## CHAOS INDICATORS: FB AND FMA

When a system is symmetric under time reversal, the numerical integration forward and backward in time can be used to indicate how sensitive the orbit is under small initial condition perturbation. It can be understood in the following way as illustrated in the Fig. 1. Consider a numerical integration forward in time. In each integration step, there is numerical error associated with the finite digits of precision. If we assume that the round-off error can be regarded as a random variable of zero mean, it will accumulate linearly with the time for regular orbits. However, for chaotic orbits

\* Work supported by the Director of the Office of Science of the US Department of Energy under Contract no. DE-AC02-05CH11231, and made use of computer resources at NERSC

<sup>†</sup> kilean@lbl.gov

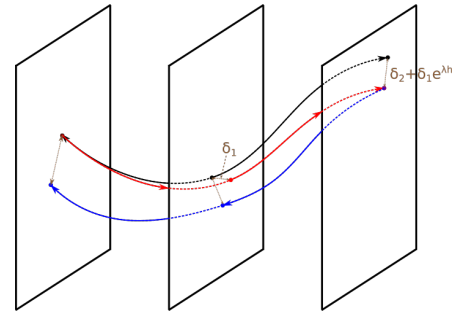


Figure 1: Illustration of FB. The planes represent the phase-space at different integration steps. The black curve is an exact orbit, red curve is the numerical integration forward in time and the blue is the numerical integration backward in time.  $\delta_i$  are numerical round off errors at  $i$ -th step,  $h$  is the integration step size, and  $\lambda$  is the growth rate which is expected to be associated with the positive Lyapunov exponents.

having positive Lyapunov exponents, the round off error can accumulate and grow exponentially. The accumulation and growth of the error can be measured by comparing the difference between the forward and backward orbit. The resolution is expected to grow exponentially over the time interval. On the other hand, the resolution of FMA depends on the measurement accuracy of the frequency, so proportional to the inverse power law of the time interval [3].

In order to quantify the indicators, we define:

$$\Delta_{FMA} \equiv \log_{10} \sqrt{\Delta v_x^2 + \Delta v_y^2}, \quad (1)$$

$$\Delta_{FB} \equiv \log_{10} \sqrt{\frac{1}{T} \sum_{t=0}^{T-1} \Delta_n(t)}, \quad (2)$$

$$\Delta_n(t) \equiv \Delta x_n^2(t) + \Delta p_{x,n}^2(t) + \Delta y_n^2(t) + \Delta p_{y,n}^2(t),$$

where  $\Delta v_x$ , and  $\Delta v_y$  are the horizontal and vertical tune differences over the successive two time intervals  $T$  and  $\Delta x_n(t)$  is the coordinate difference between the forward and backward integration at the turn number  $t$ .

## IOTA MAP MODEL

IOTA can be described by the following on-momentum Hamiltonian [4] in (dimensionless) normal coordinate  $x_n$ ,  $y_n$ ,  $p_{x,n}$ , and  $p_{y,n}$

$$H_N = \frac{1}{2} (p_{x,n}^2 + p_{y,n}^2 + x_n^2 + y_n^2) - \tau U, \quad (3)$$

where  $\tau$  is the (dimensionless) strength of the nonlinear potential and with  $z \equiv x_n + iy_n$ ,

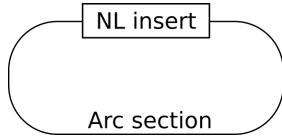


Figure 2: Schematic layout of IOTA ring.

$$U = \Re \left[ \frac{z}{\sqrt{1-z^2}} \sin^{-1}(z) \right]. \quad (4)$$

Another invariant of motion independent of  $H_N$  is

$$I_N = \frac{1}{2} (x_n p_{y,n} - y_n p_{x,n})^2 + p_{x,n}^2 + x_n^2 - \tau W, \quad (5)$$

where

$$W = \Re \left[ \frac{z + z^*}{\sqrt{1-z^2}} \sin^{-1}(z) \right]. \quad (6)$$

Note that the invariants are symmetric under the reflection  $(x_n, p_{x,n}) \rightarrow (-x_n, -p_{x,n})$  and  $(y_n, p_{y,n}) \rightarrow (-y_n, -p_{y,n})$ . The map of an autonomous Hamiltonian can be written as

$$\mathcal{N} = e^{-2\pi\nu H_N}, \quad (7)$$

where  $2\pi\nu$  is the phase-advance representing the length of the nonlinear potential element. Due to the reflection symmetry of the two invariants, the integrability is destroyed when the map is concatenated by a linear rotation map  $\mathcal{R}$  as long as the rotating angle is  $\mu\pi$  with  $\mu \in \mathbb{Z}$ . Thus

$$\mathcal{R} = e^{-\pi\mu H_R} \quad (8)$$

where

$$H_R = \frac{1}{2} (p_{x,n}^2 + p_{y,n}^2 + x_n^2 + y_n^2) \quad (9)$$

is a linear rotation Hamiltonian. The concatenated map  $\mathcal{M} = \mathcal{N}\mathcal{R}$  models the actual layout of the IOTA ring which consists of the nonlinear magnet insert section represented by  $\mathcal{N}$  and the linear arc section represented by  $\mathcal{R}$  as shown in Fig. 2.

## SIMPLIFIED SPACE-CHARGE TOY MODEL

Space-charge force perturbs both map  $\mathcal{N}$  and  $\mathcal{R}$ . Since the linear arc section is much longer than the nonlinear magnet insert section, the perturbation on  $\mathcal{R}$  is expected to be much stronger than the perturbation on  $\mathcal{N}$ . In this regard, we model space-charge effect by small perturbation  $\delta\mu$  added on the phase advance  $\mu$  over the linear arc section disregarding the nonlinear perturbation.

Figure 3 shows dynamic aperture with color map based on  $\Delta_{FMA}$  and  $\Delta_{FB}$  for  $T = 1024$ . When  $\delta\mu = 0$ , the system is perfectly integrable. However, presence of the numerical noises can break some of the invariant tori. Initial conditions of the broken tori is likely the bright region indicated by FMA and FB in common. These are the two big symmetric arcs denoted by a and two small circles near the singular points denoted by c. Arc a is understood and will

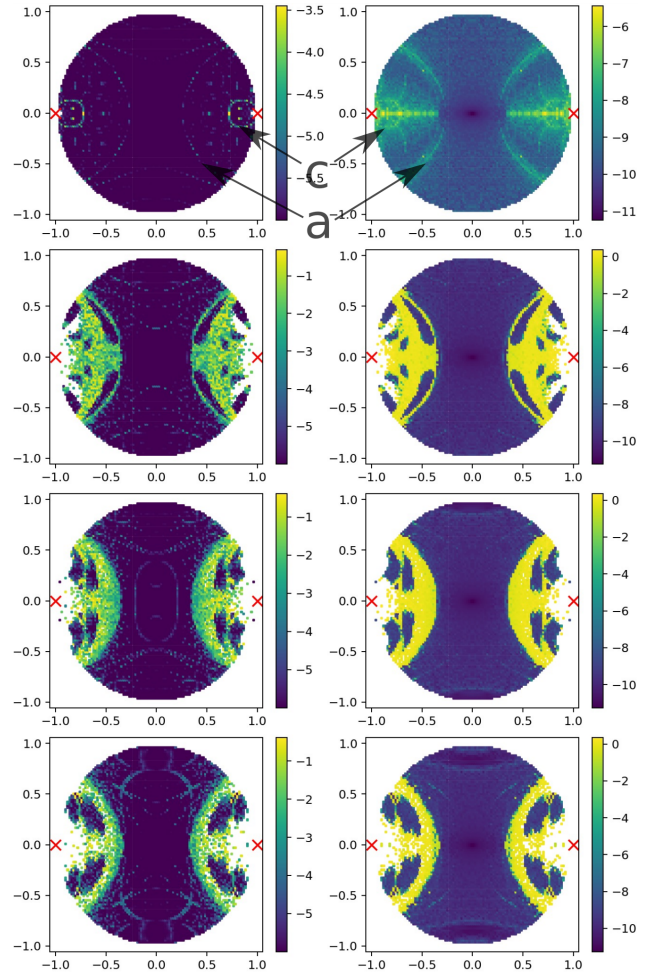


Figure 3: Dynamic aperture plot. x-y axis is the dimensionless normal coordinates  $x_n$ - $y_n$ . The color map of the left and right column are  $\Delta_{FMA}$ , and  $\Delta_{FB}$  respectively. From top to bottom  $\delta\mu$  is increasing from 0.0 to 0.03 by 0.01. Red x-marks are the singular points of the nonlinear insert potential. The time interval is  $T = 1024$ .

be discussed in future paper. It persists when  $\delta\mu \neq 0$  also as long as the perturbation is reasonably small, while the width of the arc is widening and thus gradually reducing dynamic aperture as the perturbation strength increases. Note that the FMA is more sensitive, resulting richer micro-structure compared to FB. Otherwise FMA and FB agree well. The sensitivity of FMA is also reported in [5] and explained by presence of resonant orbit. Most of such micro-structure vanishes as we sample data for longer time, as shown in Fig. 4. Furthermore, most of the particles in chaotic region previously indicated by Fig. 3 are lost in Fig. 4.

Figure 5 compares FMA and FB with various time intervals at  $\delta\mu = 0.01$ . It shows fast convergence of FB compared to FMA. In case of FB, small time interval  $T = 128$  already shows converging structure while it is not enough for FMA.

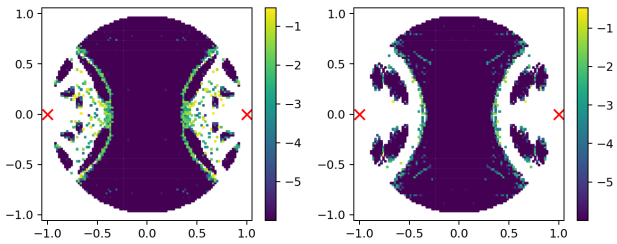


Figure 4: FMA Dynamic aperture plot with long time interval  $T = 65536$ . x-y axis is  $x_n-y_n$ . Left  $\delta\mu = 0.01$ . Right  $\delta\mu = 0.03$ .

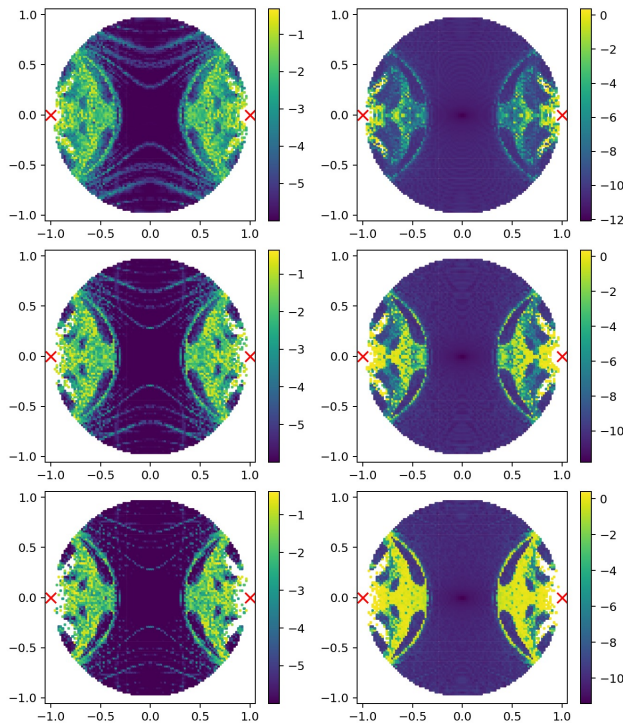


Figure 5: Comparison of FMA and FB for various  $T$  at  $\delta\mu = 0.01$ . x-y axis is  $x_n-y_n$ . Left and right column are FMA and FB respectively. From top to bottom  $T = 128, 256, 512$ .

## REALISTIC SELF-CONSISTENT SPACE-CHARGE SIMULATION

Here, we apply FMA and FB on simulation data of realistic IOTA lattice with 2D symplectic space-charge solver [6]. We choose 2D solver in order to isolate transverse space-charge effect avoiding off-momentum effect which can be induced by longitudinal space-charge force. One million macro-particles are used to represent nonlinearly matched (to the nonlinear insert potential with correction considering linear space-charge force) beam to the nonlinear potential to minimize shot-noise effect. The beam current is chosen  $I = 0.41$  mA such that the coherence tune depression is  $\delta\nu_{x,y} = -0.03$ .

Figure 6 shows dynamic aperture on realistic IOTA lattice with space-charge with  $T = 256$ . As is the case of IOTA toy models, the arc is persistent and is the major limiting structure of the dynamic aperture. The micro-structure of FMA

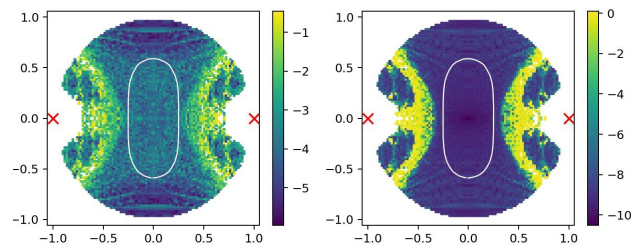


Figure 6: Comparison of FMA and FB on realistic IOTA lattice with 2D space-charge. x-y axis is  $x_n-y_n$ . Left and right column are FMA and FB respectively. The time interval is  $T = 256$ . The white contour is where the beam core reside (normalized emittance is  $\epsilon_n = 6.1 \mu\text{m}$ ).

present as well and makes the plot noisy as  $T$  is small. The beam core resides in the regular orbit and none of the particles in the beam core are lost. Note that it agrees mostly with the  $\delta\mu = 0.03$  case of Fig. 3. This is a pleasant agreement and can be understood in the following way. The lattice is matched to the coherent space-charge tune depression. This means that the bare lattice without space-charge corresponds effectively to the toy model of  $\delta\mu = 0.03$ . Therefore, particles at beam center undergo integer tune advance across the linear arc section while particles outside of the beam core has  $\delta\mu = 0.03$ .

## CONCLUSION

The forward and backward chaos indicator is compared with the frequency map analysis for IOTA ring dynamic aperture study with space-charge. The forward and backward converged faster than the frequency map analysis making it suitable application for numerically heavy simulation like space-charge routine. Both indicators agree well when converged. Application on IOTA reveals a consistent structure for various perturbation strength and it plays major role in limiting dynamic aperture. Such structure is partly understood and will be published in the future. The dynamic aperture from simple toy model agreed well with realistic space-charge simulation.

## REFERENCES

- [1] V. Danilov and S. Nagaitsev, *Phys. Rev. ST Accel. Beams* **13**, 084002 (2010).
- [2] S. Antipov *et al.*, *Journal of Instrumentation* **12**, T03002 (2017).
- [3] J. Lascar, "The Chaotic Motion of the Solar System: A Numerical Estimate of the Size of the Chaotic Zones", *Icarus* **88**, 266 (1990).
- [4] C. Mitchell and J. Qiang, in *Proc. IPAC'18*, THPAK035, Vancouver, Canada (2018).
- [5] A. Valishev, S. Nagaitsev, V. V. Danilov, and D. N. Shatilov, in *Proc. IPAC'12*, TUPPC090, New Orleans, USA (2012).
- [6] Ji Qiang, *Phys. Rev. ST Accel. Beams* **20**, 014203 (2017).